Surrogate-Based Analysis and Optimization for the Design of Heat Sinks With Jet Impingement

Xueguan Song, Jie Zhang, *Member, IEEE*, Sanghoon Kang, Mingyao Ma, Bing Ji, *Member, IEEE*, Wenping Cao, *Senior Member, IEEE*, and Volker Pickert, *Member, IEEE*

***Abstract*— Heat sinks are widely used for cooling electronic devices and systems. Their thermal performance is usually determined by the material, shape, and size of the heat sink. With the assistance of computational fluid dynamics (CFD) and surrogate-based optimization, heat sinks can be designed and optimized to achieve a high level of performance. In this paper, the design and optimization of a plate-fin-type heat sink cooled by impingement jet is presented. The flow and thermal fields are simulated using the CFD simulation; the thermal resistance of the heat sink is then estimated. A Kriging surrogate model is developed to approximate the objective function (thermal resistance) as a function of design variables. Surrogate-based optimization is implemented by adaptively adding infill points based on an integrated strategy of the minimum value, the maximum mean square error approach, and the expected improvement approaches. The results show the influence of design variables on the thermal resistance and give the optimal heat sink with lowest thermal resistance for given jet impingement conditions.**

***Index Terms*— Computational fluid dynamics (CFD), design optimization, global sensitivity analysis (GSA), heat sinks, impingement, surrogate.**

I. Introduction

IT IS well acknowledged that every electronic component produces heat during operation and they should be generally cooled to keep the component temperature within its limits [1]–[3]. Given the fact that the main cause of malfunction of electronic devices is due to overheating [4], heat sinks play a key role to remove the heat from the devices [5], and to keep them in healthy conditions. Without doubt, an optimized design of heat sinks would improve the reliability and cost-effectiveness of electronic devices. In the past decades, various types of cooling methods and technologies (e.g., water or oil cooling, jet impingement cooling, heat pipes, and phase-changing cooling) for the heat sinks have been developed and applied to meet the increasing electronic heat dissipation requirements [6]. Among these technologies, air cooling is the most widely used type of cooling in heat sinks due to its low cost, high reliability, and easy implementation [7]–[9]. The heat transfer between the source and sink is straightforward. First, the heat generated from the electronic device is transferred to the heat sink through conduction and then to the surrounding environment of the heat sink through convection. The convection can be achieved by either natural or forced airflow driven by jet impingement or fans. The effectiveness of heat transfer is significantly affected by: 1) the materials and interfaces of the electronic device, and the heat sink [10] and 2) thermal characteristics of the heat sink configuration and the airflow equipment (such as impinging jet or fans).

In the literature, there has been a significant amount of research work published on the heat dissipation of heat sink through experimental [11]–[13], analytical [15], [16], and numerical studies [17]–[19]. Thermal characteristics of heat sinks under jet impingement can be experimentally studied with a good accuracy. For instance, El-Sheikh and Garimella [13] experimentally investigated the enhancement of heat transfer through a variety of pin-fin heat sinks with confined air jet impingement. Maveety and Jung [14] presented a comparative investigation between experiments and numerical simulations of turbulent air impingement flow on a square pin-fin heat sink. However, experimental approaches generally require prototyping a heat sink and testing it with special equipment generating test signals with various thermal profiles, which are costly and time consuming. Alternatively, analytical methods can provide reasonable solutions if appropriate thermal models are developed. Some studies have been carried out to determine the optimal performance of plate-fins or pin-fins with or without jet impingement [20]–[26]. Among these, Park *et al*. [20] proposed an optimization method for plate-fin heat sinks with vortex generator using both computational fluid dynamics (CFD) and surrogate-based optimization method to search for the optimum geometries of the heat sinks. Understandably, analytical models may not generate accurate results as experiments and are thus limited to the design of simple heat sinks.

Over the past two decades, CFD has received a lot of attention and become a popular tool for modeling and simulating the heat transfer in electronic devices. Nonethe-

Manuscript received February 7, 2013; revised July 31, 2013; accepted October 9, 2013. Date of publication October 30, 2013; date of current version February 28, 2014. This work was supported by the Engineering and Physical Sciences Research Council for the Vehicle Electrical Systems Integration under Project EP/I038543/1. Recommended for publication by Associate Editor P. Dutta upon evaluation of reviewers' comments.

X. Song, M. Ma, B. Ji, and V. Pickert are with the School of Electrical and Electronic Engineering, Newcastle University, Newcastle NE17RU, U.K. (e-mail: xueguan.song@ncl.ac.uk; mingyao.ma@ncl.ac.uk; bing.ji@ncl.ac.uk; volker.pickert@ncl.ac.uk).

J. Zhang is with the Multidisciplinary Design Optimization Laboratory, Syracuse University, Syracuse, NY 13244 USA. He is currently with the National Renewable Energy Laboratory, Golden, CO 80401 USA (e-mail: jzhang56@syr.edu).

S. Kang is with the Department of Mechanical Engineering, Dong-A University, Busan 604-714, Korea (e-mail: shinji2778@hotmail.com).

W. Cao is with the School of Electronics, Electrical Engineering and Computer Science, Queen's University Belfast, Belfast BT9 5BN, U.K. (e-mail: w.cao@qub.ac.uk).

Color versions of one or more of the figures in this paper are available online at http://ieeexplore.ieee.org.

Digital Object Identifier 10.1109/TCPMT.2013.2285812

less, CFD simulation-based optimization is computationally demanding due to a large number of repeated CFD analyses, posing a particular challenge in handling highly nonlinear and implicit functions (between the thermal performance and design variables), as in the case of heat sinks. In order to overcome this obstacle, one of the practical approaches is to construct approximate models for the prediction and optimization purposes. Surrogate models, such as quadratic response surface model (RSM) [27], Kriging [28], [29], and radial basis functions [30], have been widely used for engineering optimization, which approximate the expensive numerical simulations and experiments using mathematical functions. Therein, RSM and Kriging models (KRGs) have been used for the design optimization of heat sinks [24]–[26], which are also the focus of this paper. Nevertheless, existing surrogate-based optimization methods used for optimization of heat sinks and related components are limited to one-shot experimental design, which results in that the search procedure can lead to inaccurate optima, as these surrogate models are generally constructed on the sample data generated from the initial and sole design of experiments (DoEs). Therefore, a large number of initial samples are required in order to achieve a reasonable accuracy of the optimization. In this paper, a design process combining surrogate modeling and sequential sampling strategy is proposed for the optimization of plate-fin heat sinks under jet impinging conditions. This sequential design approach with iterative construction of the surrogate model is used to ensure the suitable number and distribution of the sampling points. This generally involves two steps: 1) generating a set of initial sample points and 2) adding one or more sequential infill points in each iteration. The infill points are generated based on the sampling data and the optimization result in the previous iteration. The sequential design approach can effectively improve the traditional one-shot experimental design by reducing the number of sample points required.

II. Thermal Analysis of Heat Sinks

A. Thermal Performance Metrics

A heat sink is a device that facilitates the heat exchange between a heat source (e.g., a processor or a chip) and its surrounding environment. In order to systematically study and optimize the thermal performance of the heat sink, it is essential to first define appropriate metrics as an evaluation criteria. In this paper, the thermal resistance of the heat sink is chosen as a refinement parameter, since this is a key parameter to indicate the heat sink's thermal characteristics and thus the cooling effectiveness [11]–[21]. Thermal resistance is given by

$$R_{\text{th}} = \frac{T_{\text{avg}} - T_{\text{ref}}}{Q} \tag{1}$$

where R_{th} is the thermal resistance of heat sink (ºC/W), T_{avg} is the average temperature of the base attached on the heat sink, T_{ref} is the ambient temperature as well as the jet impingement, and Q is the thermal power dissipated by the chip for a given temperature difference. The lower the thermal resistance, the more heat can be transferred through the heat sink.

B. Numerical Models

The heat transfer through a heat sink with jet impingement involves the prediction of fluid flow and heat transfer behaviors. In forced convection, it is effective to enhance heat transfer by increasing the surface area and optimizing the free stream velocity [31]. In order to model the complex component, three-dimentional (3-D) steady Reynolds-averaged Navier–Stokes (RANS) equations and the energy equations are solved numerically. Four assumptions are applied to model the heat transfer, which are as follows: 1) the flow is turbulent and incompressible; 2) the flow is in a steady state; 3) the buoyancy and radiation heat transfer are neglected; and 4) the thermophysical properties of the fluid are temperature independent. Based on the above approximations, the governing equations (continuity, momentum, and energy equations) are established in

$$\frac{\partial(\rho u_i)}{\partial x_i} = 0 \tag{2}$$

$$\frac{\partial(\rho u_i u_j)}{\partial x_j} = -\frac{\partial p}{\partial x_i} + \frac{\partial}{\partial x_j}\left[\mu\left(\frac{\partial u_i}{\partial x_j} + \frac{\partial u_j}{\partial x_i} - \frac{2}{3}\frac{\partial u_k}{\partial x_k}\delta_{ij}\right)\right] + \frac{\partial}{\partial x_j}\left(-\overline{\rho u_i' u_j'}\right) \tag{3}$$

$$\frac{\partial(u_i(\rho E + p))}{\partial x_j} = \frac{\partial}{\partial x_j}\left[\lambda_{\text{eff}}\frac{\partial T}{\partial x_j} + u_i\left(\tau_{ij}\right)_{\text{eff}}\right] + S_E \tag{4}$$

where ρ is the fluid density and it remains constant in the differential equations as the flow is assumed to be incompressible, u_i is the velocity component, p is the static pressure, μ is the molecular viscosity (also referred to as the dynamic viscosity), δ_{ij} is the Kronecker delta function, E is the total energy per unit mass, S_E is the energy generation rate per unit volume, T is the temperature, u_i'represents the velocity fluctuation,$-\overline{\rho u_i' u_j'}$ is the Reynolds stress, λ_{eff} is the effective thermal conductivity, and $(\tau_{ij})_{\text{eff}}$ is the deviatoric stress tensor in

$$-\overline{\rho u_i' u_j'} = \left(\tau_{ij}\right)_t = \mu_t\left(\frac{\partial u_i}{\partial x_j} + \frac{\partial u_j}{\partial x_i} - \frac{2}{3}\frac{\partial u_k}{\partial x_k}\delta_{ij}\right) - \frac{2}{3}\rho k\delta_{ij} \tag{5}$$

$$\lambda_{\text{eff}} = \lambda + \lambda_t = \frac{\mu C_p}{\text{Pr}} + \frac{\mu_t C_p}{\text{Pr}_t} \tag{6}$$

$$\left(\tau_{ij}\right)_{\text{eff}} = \tau_{ij} + \left(\tau_{ij}\right)_t = \mu\left(\frac{\partial u_i}{\partial x_j} + \frac{\partial u_j}{\partial x_i} - \frac{2}{3}\frac{\partial u_k}{\partial x_k}\delta_{ij}\right) + \mu_t\left(\frac{\partial u_i}{\partial x_j} + \frac{\partial u_j}{\partial x_i} - \frac{2}{3}\frac{\partial u_k}{\partial x_k}\delta_{ij}\right) - \frac{2}{3}\rho k\delta_{ij} \tag{7}$$

where μ_t is the eddy viscotity, also referred to as the turbulent viscosity, and k is the kinetic energy of turbulence $k = 1/2\overline{u_i' u_i'}$. The parameters λ and λ_t are the laminar thermal conductivity and turbulent eddy thermal conductivity, respectively; and P_r is the Prandtl number. These equations are not closed and turbulence models are required to model the unknown Reynolds-stress tensor. To this end, the shear-stress-transport (SST) model is adopted in this paper. The SST model combines the robustness of $k-\omega$ turbulence model near walls and the capabilities of the $k-\varepsilon$ model away from the walls as a unified two-equation turbulence model. The definition of the turbulent viscosity is modified to account for the transport

of turbulent shear stress. The equations of the SST turbulence model are as follows:

$$\frac{\partial\left(\rho u_j k\right)}{\partial x_j} = \frac{\partial}{\partial x_j}\left[\left(\mu + \sigma_k \mu_t\right)\frac{\partial k}{\partial x_j}\right] + P_k - \beta^* \rho k \omega \quad (8)$$

$$\frac{\partial\left(\rho u_j \omega\right)}{\partial x_j} = \frac{\partial}{\partial x_j}\left[\left(\mu + \sigma_\omega \mu_t\right)\frac{\partial \omega}{\partial x_j}\right] + \frac{\alpha}{\upsilon_t} P_k - \beta \rho \omega^2 + 2\left(1 - F_1\right)\frac{\rho \sigma_{\omega 2}}{\omega}\frac{\partial k}{\partial x_j}\frac{\partial \omega}{\partial x_j}. \quad (9)$$

In (8) and (9), F_1 is the blending function, which activates the $k-\omega$ model in the near wall region and the $k-\varepsilon$ model for the rest of the flow and P_k is the strain-based production term $P_k = \left(\tau_{ij}\right)_t \partial u_i / \partial x_j$. All constants are computed by a blend from the corresponding constants of the k $-\varepsilon$ and k $-\omega$ model via SST = F_1 (k $-\omega$ model) + (1 $-\mathrm{F}_1$)(k $-\varepsilon$ model) [32], [33].

The thermal transfer through the heat sink is also a conjugate heat transfer problem, which involves heat conduction and forced convection, thereby the governing equation of the solid is also required

$$\frac{\partial}{\partial x_j}\left(\lambda_s \frac{\partial T}{\partial x_j}\right) + S_E = 0 \quad (10)$$

where λ_s is the thermal conductivity of the solid and T is the temperature.

III. Sequential Surrogate Modeling

For surrogate model-based optimization, the accuracy of a surrogate model is of prime importance that relies on the sampling strategy, the number, and the locations of sampling points. Therefore, the utilized sampling strategy should have the ability to generate initial sample points and to add infill points in the appropriate design domain. Kriging is a widely used surrogate modeling method in design optimization, which is adopted in this paper. The following is a brief description of the Kriging surrogate model and the sequential sampling strategy.

A. Kriging Models

The Kriging model was originally developed for mining and geostatistical applications involving spatially and temporally correlated data. The Kriging model postulates a combination of a global model combined with departures

$$y(\mathbf{x}) = f(\mathbf{x}) + Z(\mathbf{x}) \quad (11)$$

where $y(\mathbf{x})$ is the unknown function of interest, $f(\mathbf{x})$ is a known function of $\mathbf{x}$ (similar to the polynomial function in the response model, which provides a global trend of the design space), and $Z(\mathbf{x})$ represents the stochastic process with a zero mean and a nonzero variance σ^2, as well as a nonzero covariance to model local deviations. As such, the Kriging model interpolates the sampled data points. The covariance matrix of $Z(\mathbf{x})$ is formulated as

$$\mathrm{Cov}[Z(\mathbf{x}^i), Z(\mathbf{x}^j)] = \sigma^2 \mathbf{R}[R(\mathbf{x}^i, \mathbf{x}^\mathbf{j})] \quad (12)$$

where R is the symmetric correlation matrix with ones in the diagonal, and $R(\mathbf{x}^i, \mathbf{x}^j)$ is the correlation function between the two sampled points $\mathbf{x}^i$ and $\mathbf{x}^j$. The correlation function could be exponential, Gaussian, cubic, or other types of functions. In this paper, the Gaussian correlation function is employed

$$R(\mathbf{x}^i, \mathbf{x}^j) = \exp\left[-\sum_{k=1}^{\mathrm{n_{dv}}} \theta_k \left|x_k^i - x_k^j\right|^2\right] \quad (13)$$

where n_{dv} is the number of design variables, $\theta_k (k = 1, 2, \ldots, N)$ are the unknown correlation parameters used to fit the model, and $|x_k^i - x_k^j|$ is the distance between the k^{th} component of sample points $\mathbf{x}^i$ and $\mathbf{x}^j$. Once the correlation function is selected, the estimate $\hat{y}(\mathbf{x})$ of the response $y(\mathbf{x})$ at test points of $\mathbf{x}$ is given as

$$\hat{y}(\mathbf{x}) = \hat{\beta} + \mathbf{r}^T(\mathbf{x})\mathbf{R}^{-1}(\mathbf{y} - \mathbf{f}\hat{\beta}) \quad (14)$$

where $\mathbf{y}$ is the column vector of length n_s that contains the sample values of the response, and $\mathbf{f}$ is a column vector of length n_s that is filled with ones when $f(\mathbf{x})$ is taken as a constant. The term $\mathbf{r}^T(\mathbf{x})$is the correlation vector between an untried $\mathbf{x}$ and the sampled points

$$\mathbf{r}^T(\mathbf{x}) = \left[R(\mathbf{x}, \mathbf{x}^1), R(\mathbf{x}, \mathbf{x}^2), \ldots, R(\mathbf{x}, \mathbf{x}^{n_s})\right]^T \quad (15)$$

and $\hat{\beta}$ is estimated as

$$\hat{\beta} = (\mathbf{f}^T \mathbf{R}^{-1}\mathbf{f})^{-1}\mathbf{f}\mathbf{R}^{-1}\mathbf{y}. \quad (16)$$

The estimated variance of the sample data from the global model is given by

$$\hat{\sigma}^2 = \frac{(\mathbf{y} - \mathbf{f}\hat{\beta})^T \mathbf{R}^{-1}(\mathbf{y} - \mathbf{f}\hat{\beta})}{n_s} \quad (17)$$

where $f(\mathbf{x})$ is assumed to be the constant $\hat{\beta}$. The maximum likelihood estimates for θ_k in (17) used to fit the model can be determined by solving the following maximization problem over the interval $\theta_k > 0$

$$\max . \left(-\frac{n_s \ln(\hat{\sigma}^2) + \ln|\mathbf{R}|}{2}\right) \quad (18)$$

where $\hat{\sigma}^2$ and $|\mathbf{R}|$ are functions of θ_k.

B. Sequential Sampling Strategy

There are many types of sequential sampling approaches, and each of them has its own advantages and disadvantages. To effectively improve the sampling points for the approximation, three sequential sampling methods are simultaneously used in this paper, which are the minimum value approach, the maximum MSE approach, and the expected improvement approach

$$\text{Minimize } \hat{y}(\mathbf{x}) \quad (19)$$

$$\text{Maximize MSE} = \hat{y}(\mathbf{x}) \quad (20)$$

$$\text{Maximize EI} = \int_{I=0}^{I=\infty} I\left\{\frac{1}{\sqrt{2\pi}\sigma(\mathbf{x})}\exp\left[1\frac{\left(y_{\min} - I - \hat{y}(\mathbf{x})\right)^2}{2\sigma^2(\mathbf{x})}\right]\right\}. \quad (21)$$

It is worth noting that it is possible to generate new infill sampling points, which are close to the existing points or other

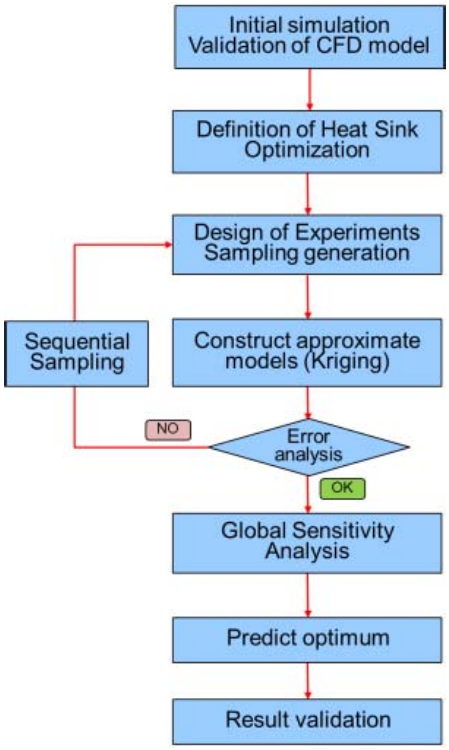

Fig. 1. Flowchart of the surrogate-based optimization procedure.

new infill points using the three approaches simultaneously. To avoid this problem, a distance constraint is introduced to exclude those new infill points which are extremely close to existing points

$$\left\|\mathbf{x}_{\text{new}}^{j}-\mathbf{x}^{i}\right\|\geq\varepsilon_1\quad(j=1,\ldots,n_{\text{new}};\ i=1,\ldots,(n_s+j-1)) \tag{22}$$

where $\mathbf{x}_{\text{new}}^{j}$ is the j^{th} new infill point obtained in terms of above three equations, $\mathbf{x}^{i}$ is i^{th} set of existing points, which includes the initial n_s sampling points and new $(j-1)$ valid points. The parameter $\varepsilon_1$is a small constant, which is defined as

$$\varepsilon_1=\frac{\|\mathbf{x}_L-\mathbf{x}_U\|}{n_s+j-1} \tag{23}$$

where $\mathbf{x}_L$ and $\mathbf{x}_U$ are the lower and upper bounds of the design variables, respectively. To effectively take advantage of this strategy with less iteration, (19) and (21) are solved by a particle swarm optimization algorithm, which is a derivative-free global optimum algorithm. Equation (20) is solved using sequential quadratic programming, which is a gradient-based approach.

C. Optimization Procedure

The overall optimization procedure is shown in Fig. 1. It begins with the initial simulation, aiming to collect information and validate the computational model. Following the validation of computational model, the next step is to conduct the heat sink optimization. Having defined the heat sink design problem, initial sampling points are generated using a Latin hypercube sampling (LHS) approach, which is one of the most widely used DoE methods. An initial approximate model is conducted using Kriging, and then the error analysis of the approximate model is carried out for assessing the accuracy of the created model. If the stop criterion is not satisfied, sequential sampling is carried out to add infill points into the design domain and then the surrogate model is updated. The surrogate-based optimization process will stop if the error is smaller than the predefined convergence tolerances. A global sensitivity analysis (GSA) is then performed to identify the significance of each design variable. When an optimum design is found, the CFD simulation is carried out again to verify the optimum design.

IV. Design Optimization of Heat Sink With Jet Impingement

A. Initial Simulation

Fig. 2 shows the geometry and the computational model used for the thermal analysis of the initial plate-fin heat sinks. Taking advantage of the symmetrical geometry, only a quarter of the heat sink and of the enclosure is modeled and simulated. In detail, it comprises an impinging jet and a plate-fin heat sink enclosed in the air domain. The cooling air is imposed at the jet nozzle with a radius (R) of 4 mm. The impingement distance (Y) between the nozzle and the tip of the fins is set to 64 mm. The plate-fin heat sinks are designed as an array of 6×2 with a cutoff gap of width (G) 4.6 mm in the x-direction. The length and width (L) of the base of the heat sinks are both 80 mm, and the thickness (b) is 8 mm. The width of the fins (W) is 9.5 mm, and the height of the fins (H) is 30 mm. To accelerate the computations, the 1/4 model of the fluid field is further broken into three domains as shown in Fig. 2. Fluid domain 1 with the jet nozzle can be used for all computations for the optimization; fluid domain 2 containing the heat sink can be modified for each special design. Fluid–fluid interface is used to connect the two fluid domains, and fluid–structure interface (FSI) is built to transfer the heat between fluid and solid domains. Grid independence has been examined, where the grid of fluid domain1 has 182 791 nodes, fluid domain 2 has 371 833 nodes, and the solid domain has 69 762 nodes. At the jet nozzle, a uniform velocity of 29.42 m/s, which corresponds to the Reynolds number of 15 000, has been imposed and the turbulence intensity is kept at 5%. The total heat source is defined as 25 W at a 40 mm $\times$ 40 mm plane at the central bottom of the heat sink, so $25/4=6.25$ W is given for the quarter model. The perimeter and the bottom of the base are thermally insulated. Smooth wall conditions have been implemented over the heat sink wall. High Resolution advection scheme is set to calculate the advection terms, and the convergence criteria are satisfied if the root mean square (RMS) residual is $<10^{-5}$.

Fig. 3 shows the velocity streamline from the nozzle and the temperature distribution on the heat sink. It is observed that most of the airflow flows out through the middle passage in the z-direction. For the channels in the x-direction, less air flows out through the second channels compared with that through the first channel, and there is the least air flowing out through the third channels. As a result, the minimum temperature of 33.589 ºC occurs on the inner tip of the center

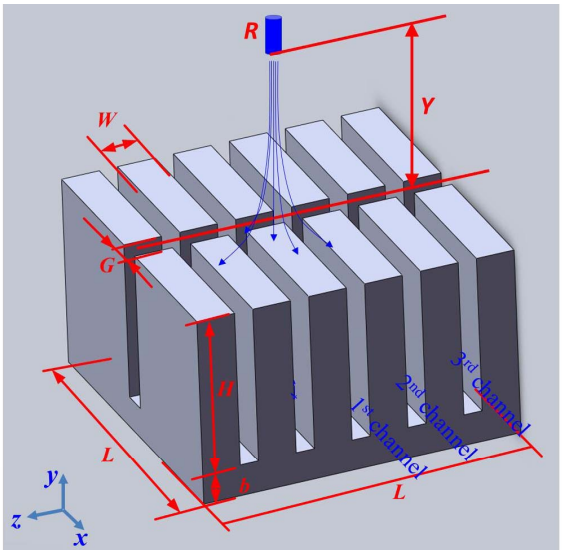

(a)

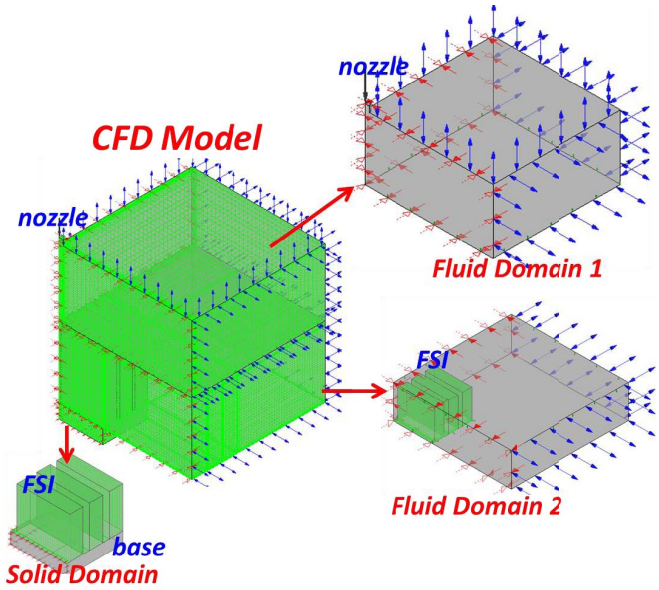

(b)

Fig. 2. Geometry and CFD model of the heat sink. (a) Geometry of heat sink with jet impingement. (b) CFD model of heat sink.

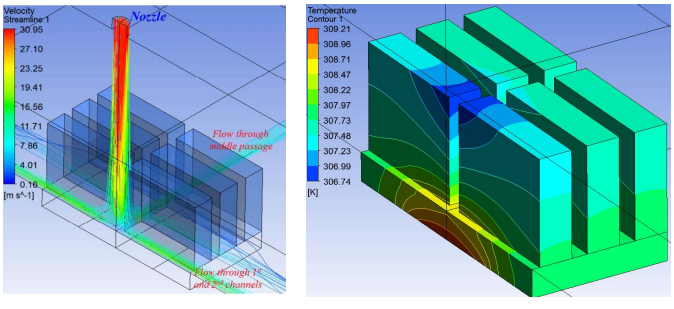

(a) (b)

Fig. 3. CFD simulation result of the base design. (a) Velocity streamline from inlet. (b) Temperature on heat sink.

fins, and the maximum temperature of 36.057 ºC occurs in the center bottom of the heat sink. The average temperature of the base is 35.742 ºC, and the maximum temperature difference on the base is only 0.968 ºC; this is because that hot spots and transient problems are not considered in this paper, and it is thus assumed that the heat power defined in the simulation is uniformly distributed on the base surface. Therefore, improving the thermal resistance derived from the average temperature rather than the maximum temperature or temperature at a specific fixed point is reasonable. Table I compares R_{th} obtained from CFD analysis and experimental research [17]. The small error indicates that the CFD model with multiple domains and SST turbulence model is sufficiently accurate for the simulation of the heat sink under jet impingement. In addition, it is shown that the dimension of fins has a significant cooling effect on the heat dissipation, as it not only impacts on the heat transfer area of the heat sink, but also influences the flow field in the heat sink. Hence, optimizing the dimension of the heat sink will be useful to improve the cooling performance.

TABLE I
CFD RESULTS COMPARED WITH EXPERIMENTAL RESULTS

Shape dimensions (mm)				R_{th} (°C/W)		
H	G	W	b	Experiments [17]	CFD results	Error (%)
30.0	4.6	9.5	8.0	0.544	0.549	0.919

B. Optimization Formulation

In theory, a lower thermal resistance of the heat sink means a better cooling performance, so the thermal resistance (R_{th}) is set as the design objective. The total size of the heat sink is generally constrained in a specific volume, i.e., only the interior dimensions can be adjusted to meet the heat transfer requirements. Therefore, the length and width of the heat sink $L \times L$ are fixed in this case, then four dimensions H, G, W, and b are selected as the design variables; the width of each channel can thus be calculated as $(L - nW)/(n - 1)$. Given that the most common heat sink material is aluminum alloy and its price is fairly low, the material of the heat sink as well as the price/weight of the heat sink is not considered in this paper. The ranges of the design variables (H, G, W, b) are defined based on [18] and [19], but are greater than those in the previous work, which allows a greater search domain for the potential optimum design. The optimization problem can be mathematically defined as

$$\begin{aligned} &\text{find} \quad X = (H, G, W, b) \\ &\begin{cases} \text{Minimize} \quad R_{\text{th}} = f(X) \\ s.t. \quad \begin{cases} 20 \text{ mm} \le H \le 60 \text{ mm} \\ 1 \text{ mm} \le G \le 20 \text{ mm} \\ 5 \text{ mm} \le W \le 13 \text{ mm} \\ 2 \text{ mm} \le b \le 16 \text{ mm}. \end{cases} \end{cases} \end{aligned} \tag{24}$$

C. Test Results

The initial Kriging model is constructed based on 28 sample points generated using the LHS approach. Two loops of sequential sampling approach have been carried out according to (19)–(23), where nine new infill points are supplemented

TABLE II
VALIDATION OF INITIAL AND SEQUENTIAL KRIGING MODELS

Kriging model	n_s	Error	
		Max. error	RMSE
Initial	28	0.080	0.063
1st sequential	28+9	0.056	0.014
2nd sequential	28+9+5	0.031	0.011

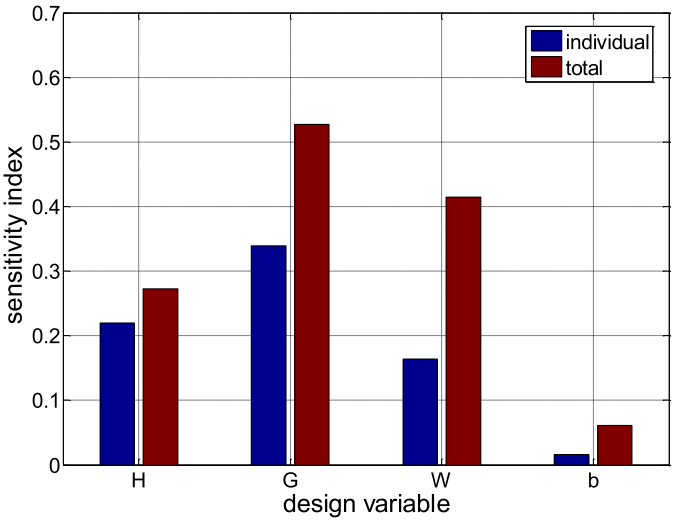

Fig. 4. Individual and total sensitivity index of design variables.

in the first loop and another five infill points are added in the second loop. Among the 14 infill points, two sequential sampling points are obtained based on (19) and (21); the other 12 points are obtained using (20). It is found that most of the points are scattered on the frontier of the design variables. This is because the initial 28 points generated with LHS are scattered within the bounds of the design variables and thereby the surrogate accuracy is relatively low in the regions close to the boundaries. Table II lists the maximum absolute error and the root mean square error (RMSE) of the initial Kriging surrogate with the 28 sampling data and sequential Kriging models by comparing the predicted results and reanalyzed results at five randomly generated validation points. It is observed that as more sampling points are added, the sequential model becomes more accurate, the maximum absolute error and RMSE decrease from 0.08 and 0.063 to 0.031 and 0.011, respectively. This result also indicates that the second sequential Kriging model is more accurate and is thus chosen for the sensitivity analysis and the search for optimum design.

A GSA is performed using the approximated Kriging model to identify the effect magnitude of each design variable on the thermal resistance. Sobol's method [34] is employed in this paper, where a total of 100 000 of Monte Carlo random samples are tested. Fig. 4 shows the sensitivity index of each design variable. It is seen that the most important factor is G, which has a main effect of ~33.98% and a total effect of

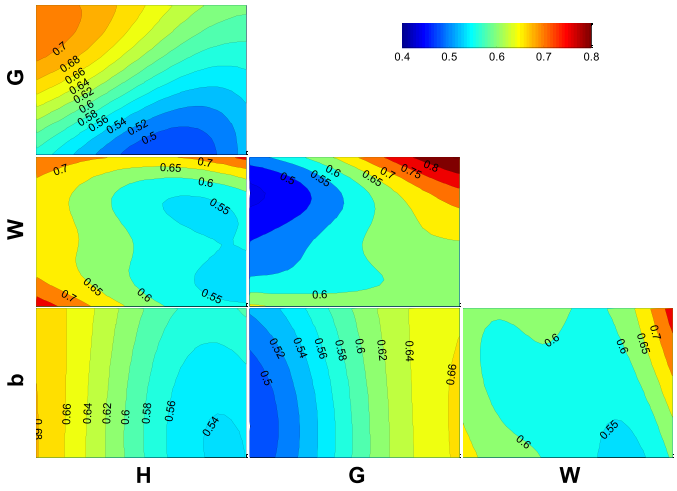

Fig. 5. Multiple plots of thermal resistance with respect to design variables.

52.29%. The second most important parameter is W, with a main effect of 18.40% and a total effect of 40.01%. The third most important variable is H, which has a main effect of 23.24% and a total effect of 26.35%. In addition, compared with the three variables, the change in width b has little effect on the thermal resistance, which is only 5.38% in the main effect and 6.27% in the total effect. It can be inferred from the results that the total heat transfer area is still the key factor for the heat sink under jet impingement. Nevertheless, the fact that G is more important than W suggests that the air flow path is also very crucial for a heat sink under jet impingement condition. The large difference between the individual sensitivity index and total sensitivity index of G and W implies that they may have significant interactive effect on the flow path as well as thermal resistance.

Fig. 5 shows the contour plots of the thermal resistance. Each subplot shows the effect of two design variables with remaining variables kept at the baseline values, which are the averages of the upper and the lower bounds of the corresponding variables. The effect importance of design variables on the thermal resistance is consistent with results in Fig. 4; design variables G and H are much more pronounced for the thermal resistance and the thickness b only has a considerable effect while comparing to W. It is seen from the H–b subplot that thermal resistance can be decreased by increasing H and decreasing b if G and W are both fixed; this is because decreasing b can reduce the thermal resistance of the base, and increasing H can effectively increase the total heat transfer area. However, this trend is not always valid for large H as seen from the H–W and H–G subplots. This is because the increase in H adds flow resistance to the air flowing to the bottom of heat sink. Similar results can also be observed for W in the G–W subplot when the H and b are fixed. W should be kept at the modest level to prevent blockage of flow path while gaining a lower thermal resistance. While the thermal resistance is seen to rapidly decrease when G approaches its lowest level, which can be attributed to the increase of the total heat transfer area and the decrease of the spread thermal resistance as the heat source is placed on the center of the bottom. Even b has little influence on the

TABLE III
OPTIMUM DESIGN OF THE HEAT SINK

	H	G	W	b	R_{th}
Base design	30.0	4.6	9.5	8.0	0.549
Optimum design	47.3	1.0	11.9	14.1	0.456
Reduction (%)	-57.7	78.3	-25.3	-76.3	16.9

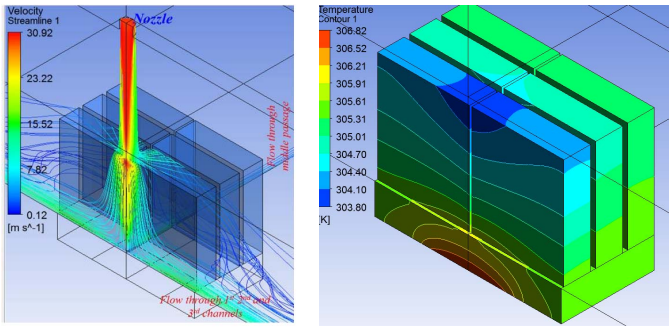

(a) (b)

Fig. 6. CFD simulation result of the optimum design. (a) Velocity streamline from inlet. (b) Temperature on heat sink.

thermal resistance as shown in Fig. 4 and all b-related subplots, it need to be taken into account carefully as its effect differs from that in a unpinned heat sink. It should be noticed that each subplot in Fig. 5 shows the thermal resistance with other two design variables fixed at the baseline values, simultaneous consideration of these four design variables as well as the optimization is thus complicated.

The optimum design is obtained using the surrogate-based optimization and listed in Table III for comparison. It is observed that the thermal resistance decreases by ∼16.9% as compared with the base design. The result is consistent with the GSA result that is discussed previously, the dimension combination with the smallest G, higher b, and modest W and H are the optimum design for the heat sink under jet impingement. Fig. 6 further illustrates the velocity streamlines through the optimum heat sink and the temperature distribution. Comparing with the base design in Fig. 3, it is seen that the flow reaches the bottom of the heat sink without any dispersion in the base design, so the heat can be removed promptly and directly from the base plate. On the contrary, the air flow is seen to be blocked and dispersed to the second channel in the optimum design as the cutoff gap of width G is fairly small. In theory, this causes a reduced air pressure and velocity at the base plate, resulting in a low heat transfer rate at the bottom. Nevertheless, a smaller width G reduces the spread thermal resistance around the base center as well as enhances the air convection in the first and second channels. Therefore, the total cooling performance of the optimum design is still better than the base design.

Fig. 7 shows the influence of the Reynolds number on both the base design and optimum design. The thermal resistance decreases effectively and monotonously with the increase of the Reynolds numbers. However, the decreasing ratio is

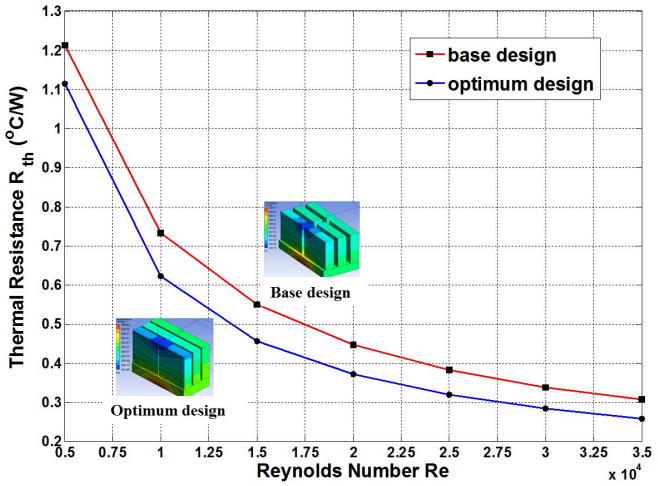

Fig. 7. Influence of the Reynolds number on the thermal resistance.

observed to decrease as the Reynolds number increases, thus a continuous increase in the Reynolds number/air velocity at the nozzle is not always effective to decrease the thermal resistance. For a specific heat sink, there exists a Reynolds number limit, over which the air flow might have no effect on the cooling performance.

V. CONCLUSION

In this paper, a novel sequential optimization approach based on Kriging was presented for the design optimization of a plant-fin heat sink under jet impingement. To study the performance and to acquire the optimal design of the heat sink, both CFD analysis and surrogate-based optimization were implemented. First, a CFD analysis was performed to simulate the heat transfer of the heat sink, and the CFD simulation performance was validated by experimental results. Second, an initial Kriging model was constructed to approximate the relationship between the four design variables and the average temperature using 28 sampling points. To enhance the accuracy of the approximation model, a sequential sampling approach was proposed to search new infill points for the final surrogate-based optimization. Last, a GSA was performed to investigate the significance of each design variable on the heat transfer performance and the relationships between the design variables and the thermal resistance. The results show that the gap width G is the most significant variables to impact on the thermal resistance of heat sink with central jet impingement. The results also show that the combination of CFD analysis and sequential surrogate model-based optimization is an effective tool for the optimal design of a heat sink under jet impingement, in conjunction with the sensitivity analysis to rank the influence of the design variables on the cooling performance.

REFERENCES

[1] L. Biswal, S. Chakraborty, and S. K. Som, "Design and optimization of single-phase liquid cooled microchannel heat sink," *IEEE Trans. Compon., Packag. Manuf. Technol.*, vol. 32, no. 4, pp. 876–886, Dec. 2009.

[2] S. G. Singh, S. P. Duttagupta, and A. Agrawal, "Real-time impact analysis of very high heat flux transients and mitigation using on-chip single-phase and two-phase microfluidics," *IEEE/ASME J. Microelectromech. Syst.*, vol. 18, no. 6, pp. 1208–1219, Jun. 2009.

[3] S. G. Singh, A. Agrawal, and S. P. Duttagupta, "Reliable MOSFET operation using two-phase microfluidics in presence of high heat flux transients," *J. Micromech. Microeng.*, vol. 21, no. 10, pp. 105002-1–105002-6, Oct. 2011.

[4] A. Sanyal, K. Srinivasan, and P. Dutta, "Numerical study of heat transfer from pin-fin heat sink using steady and pulsated impinging jets," *IEEE Trans. Compon. Packag. Technol.*, vol. 32, no. 4, pp. 859–867, Dec. 2009.

[5] A. Bar-Cohen and M. Iyengar, "Least-energy optimization of air-cooled heat sinks for sustainable development," *IEEE Trans. Compon. Packag. Technol.*, vol. 26, no. 1, pp. 16–25, Mar. 2003.

[6] C. J. M. Lasance and R. E. Simons, "Advances in high-performance cooling for electronics," *Electron. Cooling*, vol. 11, no. 4, pp. 1–13, Nov. 2005.

[7] M. B. Chaudhari, B. Puranik, and A. Agrawal, "Heat transfer characteristics of a heat sink in presence of a synthetic jet," *IEEE Trans. Compon. Packag. Technol.*, vol. 2, no. 3, pp. 457–463, Mar. 2012.

[8] C. J. Shih and G. C. Liu, "Optimal design methodology of plate-fin heat sinks for electronic cooling using entropy generation strategy," *IEEE Trans. Compon. Packag. Technol.*, vol. 27, no. 3, pp. 551–449, Sep. 2004.

[9] H. Y. Li, M. H. Chiang, and K. Y. Chen, "Performance analysis of pin-fin heat sinks with confined impingement cooling," *IEEE Trans. Compon. Packag. Technol.*, vol. 30, no. 3, pp. 383–389, Sep. 2007.

[10] A. Stupar, U. Drofenik, and J. W. Kolar, "Optimization of phase change material heat sinks for low duty cycle high peak load power supplies," *IEEE Trans. Compon., Packag., Manuf. Technol.*, vol. 2, no. 1, pp. 102–115, Jan. 2012.

[11] R. W. Knight, J. S. Goodling, and B. E. Gross, "Optimal thermal design of air cooled forced convection finned heat sinks-experimental verification," *IEEE Trans. Compon., Hybrids, Manuf. Technol.*, vol. 15, no. 5, pp. 754–760, Feb. 1992.

[12] A. Husain and K. Y. Kim, "Shape optimization of micro-channel heat sink for micro-electronic cooling," *IEEE Trans. Compon. Packag. Technol.*, vol. 31, no. 2, pp. 322–330, Jun. 2008.

[13] H. A. El-Sheikh and S. V. Garimella, "Enhancement of air jet impingement heat transfer using pin-fin heat sinks," *IEEE Trans. Compon. Packag. Technol.*, vol. 23, no. 2, pp. 300–308, Jun. 2000.

[14] J. G. Maveety and H. H. Jung, "Heat transfer from square pin-fin heat sinks using air impingement cooling," *IEEE Trans. Compon. Packag. Technol.*, vol. 25, no. 3, pp. 459–469, Sep. 2002.

[15] W. A. Khan, J. R. Culham, and M. M. Yovanovich, "Optimization of microchannel heat sinks using entropy generation minimization method," *IEEE Trans. Compon. Packag. Technol.*, vol. 32, no. 2, pp. 243–251, Mar. 2009.

[16] K. H. Do, T. H. Kima, and S. J. Kim, "Analytical and experimental investigations on fluid flow and thermal characteristics of a plate-fin heat sink subject to a uniformly impinging jet," *Int. J. Heat Mass Transfer*, vol. 53, nos. 9–10, pp. 2318–2323, Apr. 2010.

[17] A. Sanyal, K. Srinivasan, and P. Dutta, "Numerical study of heat transfer from pin-fin heat sink using steady and pulsated impinging jets," *IEEE Trans. Compon. Packag. Technol.*, vol. 32, no. 4, pp. 859–867, Dec. 2009.

[18] H. Y. Li and K. Y. Chen, "Thermal performance of plate-fin heat sinks under confined impinging jet conditions," *Int. J. Heat Mass Transfer*, vol. 50, nos. 9–10, pp. 1963–1970, May 2007.

[19] H. Y. Li, K. Y. Chen, and M. H. Chiang, "Thermal-fluid characteristics of plate-fin heat sinks cooled by impingement jet," *Energy Convers. Manag.*, vol. 50, no. 11, pp. 2738–2746, Nov. 2009.

[20] K. Park, P. K. Oh, and H. J. Lim, "The application of the CFD and Kriging method to an optimization of heat sink," *Int. J. Heat Mass Transfer*, vol. 49, nos. 19–20, pp. 3439–3447, Sep. 2006.

[21] B. Sahin and A. Demir, "Thermal performance analysis and optimum design parameters of heat exchanger having perforated pin fins," *Energy Convers. Manag.*, vol. 49, no. 6, pp. 1684–1695, Jun. 2008.

[22] K. T. Chiang, C. C. Chou, and N. M. Liu, "Application of response surface methodology in describing the thermal performances of a pin-fin heat sink," *Int. J. Thermal Sci.*, vol. 48, no. 6, pp. 1196–1205, Jun. 2009.

[23] J. H. Zhou, C. X. Yang, and L. N. Zhang, "Minimizing the entropy generation rate of the plate-finned heat sinks using computational fluid dynamics and combined optimization," *Appl. Thermal Eng.*, vol. 29, nos. 8–9, pp. 1872–1879, Jun. 2009.

[24] K. Y. Kim and M. A. Moon, "Optimization of a stepped circular pin-fin array to enhance heat transfer performance," *Heat Mass Transfer*, vol. 46, no. 1, pp. 63–74, Nov. 2009.

[25] D. Jang, S. H. Yu, and K. S. Lee, "Multidisciplinary optimization of a pin-fin radial heat sink for LED lighting applications," *Int. J. Heat Mass Transfer*, vol. 55, no. 4, pp. 515–521, Jan. 2012.

[26] N. Celik and E. Turgut, "Design analysis of an experimental jet impingement study by using Taguchi method," *Heat Mass Transfer*, vol. 48, no. 8, pp. 1407–1413, Aug. 2012.

[27] I. André, J. Khuri, and A. Cornell, *Response Surfaces: Designs and Analyses*. Boca Raton, FL, USA: CRC Press, 1996.

[28] G. Matheron, "Principles of geostatistics," *Econ. Geol.*, vol. 58, no. 8, pp. 1246–1266, 1963.

[29] S. Jerome, J. William, T. Welch, J. Mitchell, and H. P. Wynn, "Design and analysis of computer experiments," *Stat. Sci.*, vol. 4, no. 4, pp. 409–435, 1989.

[30] M. J. L. Orr, "Introduction to radial basis function networks," in *Center for Cognitive Science*. Edinburgh, U.K.: Edinburg University, 1996.

[31] A. Shah, B. G. Sammakia, H. Srihari, and K. Ramakrishna, "A numerical study of the thermal performance of an impingement heat sink-fin shape optimization," *IEEE Trans. Compon. Packag. Technol.*, vol. 27, no. 4, pp. 710–717, Dec. 2004.

[32] F. R. Menter, M. Kuntz, and R. Langtry, "Ten years of industrial experience with the SST turbulence model," *Turbulence, Heat Mass Transfer*, vol. 4, pp. 625–632, Jun. 2003.

[33] A. Horvat and Y. Sinai, *Validation of Two-Equation Turbulence Models for Heat Transfer Applications*. New York, NY, USA: Oxford, 2003.

[34] I. M. Sobol, "Global sensitivity indices for nonlinear mathematical models and their Monte Carlo estimates," *Math. Comput. Simul.*, vol. 55, nos. 1–3, pp. 271–280, Feb. 2001.

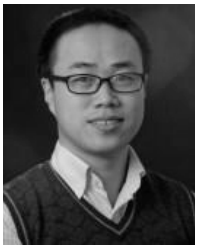

Xueguan Song received the B.S. degree in mechanical engineering from the Dalian University of Technology, Dalian, China, in 2004, and the M.S. and Ph.D. degrees in mechanical engineering from Dong-A University, Busan, Korea, in 2007 and 2010, respectively.

He is currently an EPSRC Research Associate with the School of Electrical and Electronic Engineering, Newcastle University, Newcastle Upon Tyne, U.K. He has published over 20 peer-reviewed journal papers, one book, and one book chapter in various research fields such as engineering optimization, computational fluid dynamics analysis, structural design, and thermal management. His current research interests include multidisciplinary design optimization, electronic packaging design, reliability and modeling, computational fluid dynamics, and thermal management.

Dr. Song is a recipient of the Best Paper Award at LDIA Conference in 2013, the Best Poster Awards at CSO in 2011 and PCO in 2010 Conferences, and the Honorable Mention Award in the Ph.D. Student Paper Symposium and Competition at the ASME PVP Conference in 2010.

Jie Zhang (M'13) received the B.S. and M.S. degrees in mechanical engineering from the Huazhong University of Science and Technology, Wuhan, China, and the Ph.D. degree in mechanical engineering from the Rensselaer Polytechnic Institute, Troy, NY, USA, in 2012.

He was working as a Postdoctoral Research Associate at Syracuse University. He is currently a Post-Doctoral Researcher with the Transmission and Grid Integration Group, National Renewable Energy Laboratory, Golden, CO, USA. His current research interests include multidisciplinary design optimization, wind energy, solar energy, power & energy systems modeling and simulation.

Sanghoon Kang received the B.S. and M.S. degrees in mechanical engineering from Dong-A University, Busan, Korea, in 2010 and 2012, respectively, where he is currently pursuing the Ph.D. degree in mechanical engineering.

His current research interests include design and analysis of offshore plant, design optimization of jet pump and valves.

Mingyao Ma received the B.Sc. and Ph.D. degrees in applied power electronics and electrical engineering from Zhejiang University, Hangzhou, China, in 2004 and 2010, respectively.

She was a Visiting Ph.D. Post-Graduate Research Student with the University of Strathclyde, Glasgow, U.K., from October 2008 to October 2009, and she was with Zhejiang University as a Post-Doctoral Research Fellow in 2010. In 2011, she was with the University of Central Florida, Orlando, FL, USA, as the Visiting Scholar. From April 2012, she was with Newcastle University, Newcastle Upon Tyne, U.K., as a Research Associate. Her current research interests include multilevel converters, distributed control of PEBB-based converters, software design using FPGA and DSP, and SR motor control.

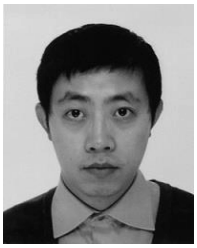

Bing Ji (M'13) received the M.Sc. and Ph.D. degrees in electrical and electronic engineering from Newcastle University, Newcastle Upon Tyne, U.K., in 2007 and 2012, respectively.

He was a Power Electronics Engineer with a U.K. Low Carbon Vehicle Company from 2012, where he worked on powertrain development and battery management system for hybrid electric vehicles. Since 2013, he has been an EPSRC Post-Doctoral Researcher with Newcastle University, where he is involved in accurate power loss measurement for high efficiency power converters and motors with calorimetric methods. His current research interests include reliability and diagnosis of power semiconductor devices, batteries and power converter systems, gate drivers, electro-thermal modeling, high-density converter integration, and thermal management for electric vehicle applications.

Dr. Ji is a member of the IEEE PELS Societies.

Wenping Cao (M'05–SM'11) received the B.Eng. degree in electrical engineering from Beijing Jiaotong University, Beijing, China, in 1991, and the Ph.D. degree in electrical machines and drives from the University of Nottingham, Nottingham, U.K., in 2004.

He is currently a Senior Lecturer with Queen's University Belfast, Belfast, U.K. His current research interests include fault analysis and condition monitoring of electric machines, drives and power electronics.

Dr. Cao serves as an Associate Editor for the IEEE TRANSACTIONS ON INDUSTRY APPLICATIONS and the IEEE INDUSTRY APPLICATIONS MAGAZINE as well as an editorial board member for nine other international journals. He is a member of the Institution of Engineering and Technology and a fellow of Higher Education Academy.

Volker Pickert (M'04) received the Dipl.-Ing. degree in electrical and electronic engineering from Rheinisch-Westfaelische Technische Hochschule, Aachen, Germany, in 1994, and the Ph.D. degree from Newcastle University, Newcastle Upon Tyne, U.K., in 1997.

He was an Application Engineer with Semikron International, Nuremberg, Germany, from 1998 to 1999, and he was a Group Leader with Volkswagen, Wolfsburg, Germany, from 1999 to 2003, and responsible for the development of electric drives for electric vehicles. In 2003, he was a Senior Lecturer within the Power Electronics, Drives and Machines Research Group, Newcastle University, and became a Professor of Power Electronics in 2011. He has published over 90 papers in the area of power electronics. His current research interests include power electronics for automotive applications, thermal management, fault tolerant converters, and advanced nonlinear control.

Dr. Pickert is a recipient of the ImarEst Denny Medal for the best journal paper in marine applications. He was a Chairman of the Biannual International IET Conference on Power Electronics, Machines and Drives in 2010. He is an Executive Steering Member with the IET PGCU Network and the Head of the PEDM Research Group.